THE JOURNAL OF PHYSICAL CHEMISTRY C

pubs.acs.org/JPCC Article

Monitoring Local Electric Fields using Stark Shifts on Napthyl Nitrile-Functionalized Silicon Photoelectrodes

Haotian Shi, Ryan T. Pekarek, Ran Chen, Boxin Zhang, Yu Wang, Indu Aravind, Zhi Cai, Lasse Jensen, Nathan R. Neale, and Stephen B. Cronin*

Cite This: J. Phys. Chem. C 2020, 124, 17000−17005

Read Online

ACCESS | Metrics & More | Article Recommendations

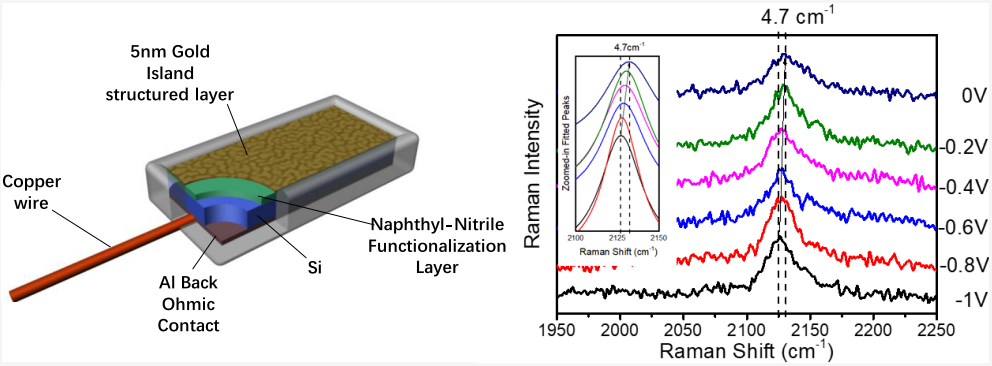

ABSTRACT: We report spectroscopic measurements of the local electric field using vibrational Stark shifts of napthyl nitrile-functionalized silicon under electrochemical working conditions. The C≡N bond is particularly sensitive to applied electric fields and serves as a good probe for the local electric fields at the silicon−aqueous interface. Here, surface-enhanced Raman spectra (SERS) are collected at a silicon surface using a water immersion lens as a function of the reference potential in a three-terminal potentiostat. In deionized (DI) water and KCl solutions, the nitrile (i.e., C≡N) stretch downshifts by 4.7 and 8.6 cm^{-1}, respectively, under an applied potential of −1 V vs Ag/AgCl. Density functional theory (DFT) calculations of the napthyl nitrile complex carried out under various electric fields establish the Stark tuning rate to be 0.5622 $cm^{-1}/(MV\ cm^{-1})$. Based on this relation, electric fields of −8.4 and −15.2 MV/cm were obtained under negative applied potentials. These measurements report the electric field strength within the double (i.e., Helmholtz) layer, which is responsible for pulling positively charged ions (e.g., H^+) toward the surface in reduction reaction processes.

INTRODUCTION

With the wide-scale adoption of silicon-based solar photovoltaics, it is important to develop scalable methods for solar energy storage to provide solar-based energy during nights, cloudy days, and winter months. Artificial photosynthesis is one of the most effective methods to store the sun's energy in chemical bonds that can later be released without producing harmful pollutants. While this general principle was demonstrated almost 50 years ago by Fujishima and Honda,[1,2] a practical method enabling silicon to remain photochemically stable was not demonstrated until 2011 with the discovery that thin films of amorphous TiO_2 deposited by atomic layer deposition (ALD) can make silicon photochemically stable without sacrificing photocatalytic performance.[3] This approach has since been applied to GaInP, GaAs, and InP, resulting in world record efficiencies in solar-driven hydrogen evolution.[4−12] While a majority of previous research in photocatalysis was based on metal oxide materials, which have low carrier mobilities/lifetimes and large band gaps, the utilization of high-quality optoelectronic materials has given way to more precise control of the energy landscapes seen by electrons as they pass through photocatalytic interfaces.[13−16] Despite this, little is known about the fundamental physics and chemistry that takes place at the semiconductor−aqueous interface, including electric fields and charge density, adsorption and deposition of species, etc.

The large electrostatic fields at electrode and photoelectrode surfaces (i.e., double layer, Helmholtz layer) play a significant role in electrochemical reactions by pulling charged or polarized reactants toward this interface.[17] Therefore, these

Received: May 4, 2020
Revised: June 28, 2020
Published: July 10, 2020

electrostatic fields strongly influence reaction mechanisms and catalysis, which are closely related to the local field strength at these interfaces. Previously, sum frequency generation (SFG) spectroscopy explored the interfacial solvation effects of 4-mercaptobenzonitrile (4-MBN) via the C−N frequency shift at gold electrode surfaces.[17,18] Lian's group also used SFG probes to probe electric fields at electrochemical interfaces.[19] While extremely surface-sensitive, SFG spectroscopy is a challenging method, mainly due to the strong IR absorption in water (electrolyte). This limits the optical path length to roughly 25-μm-thick microfluidic channels or cells. Nonlinear optical mixing of other components in the system gives rise to large background signals, which obscure the small signals generated by the surface layer of molecules.

Surface-enhanced Raman spectra (SERS)-based vibrational Stark shifts represent an easier, more widely accessible way to probe interfacial electric fields. Hildebrandt et al.[20] and Harris et al.[21,22] reported SERS-based vibrational Stark shifts of roughened metal electrodes. Shi et al. reported SERS-based Stark shifts on Au nanoisland films deposited by electron-beam evaporation, which are known to possess strong plasmon resonances.[23−27] In particular, the small gaps between the islands in these films produce intense electric field "hot spots", which produce strong SERS enhancement. These previous approaches on metal electrodes use surface-bound thiolated molecules, such as 4-MBN, as a key component of this spectroscopic approach. Electrochemical surface-enhanced Raman spectroscopy (i.e., E-SERS) has also been used to study chemical species adsorbed on metal electrode surfaces, however, many of these studies report irreversible changes in the spectra and results that have not been reproduced by other groups.[28−33] In these previous SERS-based Stark-shift studies, only the electric fields at metal electrodes were studied.

In work presented here, we probe the Stark-shifted electric fields at the surface of a silicon photoelectrode using napthyl nitrile functionalization. This work leverages the vast body of knowledge on silicon functionalization which spans a wide range of applications from micro-electromechanical systems (MEMS), microfluidics, biosensors, and other bioanalytical applications, all with different interfacial characteristics.[34−36] Previous *in situ* Raman-based Stark-shift measurements have been carried on metal electrodes (i.e., Au[37] and graphene[38]). Here, we present a strategy for monitoring local electrostatic fields at semiconductor/liquid interfaces using Stark shifts in nitrile groups measured by SERS.

EXPERIMENTAL DETAILS

Figure 1 shows a schematic diagram of the experimental setup and sample configuration. The procedure for synthesis and surface immobilization of 2-cyano-3-[4-(dimethylamino) naphthalen-1-yl] prop-2-enoic acid (**1**) was adapted from a Knoevenagel condensation published previously,[39] in which 4-dimethlyamino-1-napthaldehyde (Aldrich, 97%; 1 equiv, 5 mmol, 0.996 g) and cyanoacetic acid (Aldrich, 99%; 1 equiv, 5 mmol, 0.423 g) were dissolved in a minimum amount of ethanol (high-performance liquid chromatography (HPLC) grade, Pharmoco) and added to a round bottom flask. Next, piperidine (Aldrich, *ReagentPlus*; 0.12 mol %, 0.6 mmol, 51 mg) was added dropwise to the solution. The stirred solution was heated to reflux overnight. Afterward, the ethanol was removed under vacuum, and the remaining red solid was washed with cold methanol (J.T. Baker, Reagent Grade; 0 °C) and placed under vacuum for ∼3 h. After purification by

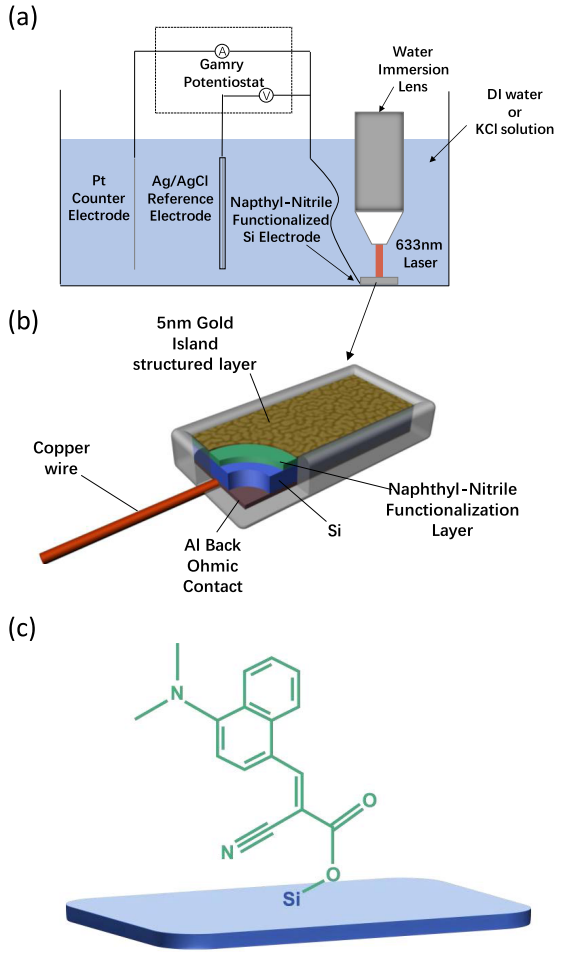

Figure 1. (a) Schematic diagrams of the three-terminal photoelectrochemical cell using a water immersion lens, (b) napthyl nitrile-functionalized Si electrode, and (c) molecular structure of the grafted silicon.

column chromatography using a silica stationary phase and ethyl acetate (J.T. Baker, reagent grade) as an eluent, the product (**1**) was bound to the silicon surface. To prepare the silicon for functionalization, a p-type silicon wafer (100-oriented, boron-doped, dopant concentration 1.0−1.5 × 10^{16} cm^{-3}, from Topsil, Inc.) was sonicated for 10 min each in acetone (electronic grade, J.T. Baker), isopropanol (Fischer), and deionized water. The oxide-terminated silicon was then etched in 2 M hydrofluoric acid (Sigma, 48% Reagent Grade, diluted with deionized (DI) water) for 60s, and immediately brought into an Ar glovebox (0.1 ppm O_2, <0.5 ppm H_2O). To chlorinate the Si−H sites on the wafer, 10 mL of chlorobenzene (Aldrich, HPLC grade, dried and distilled over CaH_2) solution saturated with phosphorus pentachloride (Fluka, >98%) and 5−10 mg of a radical initiator (1,1′-azobis(cyclohexanecarbonitrile), Aldrich, 98%) was prepared. The wafer was soaked in the chlorination solution for 1 h at 90 °C in a sealed vial. After thoroughly rinsing the wafer with chlorobenzene and toluene (J.T. Baker, reagent grade, distilled over CaH_2), the now chlorine (Cl)-terminated Si wafer was allowed to react with a saturated solution of 2-cyano-3-[4-(dimethylamino) naphthalen-1-yl] prop-2-enoic acid in dry toluene at 100 °C overnight in a sealed vial. Afterward, the wafer was rinsed thoroughly with dry toluene and sonicated (10 min) in dry toluene without exposure to air.

https://dx.doi.org/10.1021/acs.jpcc.0c03966
J. Phys. Chem. C 2020, 124, 17000−17005

Initially, after this functionalization procedure, we could not obtain enough Raman signal from the napthyl nitrile-functionalized Si to perform Stark-shift spectroscopy. To increase the Raman signal, we deposited a 5 nm (nominal thickness) Au film on the sample surface using electron-beam evaporation. Five nanometers is not enough to form a continuous film, which is known to be strongly plasmonic.[23,24,37,40] It is important to note that the napthyl nitrile molecules are bound to the silicon and not the Au nanoparticles. The structure of the sample is illustrated in Figure 1b. Then, an Ohmic back contact of 200 nm aluminum was deposited using e-beam deposition. A copper wire was attached to the ohmic back contact, and the whole sample was mounted on a glass slide and encapsulated in epoxy. This is how we made our working electrode in a three-terminal potentiostat setup.

In-situ Raman measurements of the plasmonic-enhanced, napthyl nitrile-functionalized silicon surface were taken under 633 nm wavelength excitation using our Renishaw Raman system, in pure DI water and 0.1 M potassium chloride solution using a water immersion lens, as illustrated in Figure 1a. The lens was protected from the electrolyte solution by a 13-μm-thick Teflon sheet (American Durafilm, Inc.). The electrochemical potentials were applied by our potentiostat workstation (Gamry, Inc.) with respect to the reference electrode. Silver/silver chloride (Ag/AgCl) reference electrode and platinum wires were used as the reference and counter electrodes, respectively. The exposed sample surface area was about 1 cm^2. We observed a weak Raman signal from the C≡N nitrile stretch mode around 2125.0 cm^{-1} with a 120 s integration time and 0.5 mW laser power. As such, the Au nanoisland system presents a unique opportunity to study *in-situ* SERS spectra at electrochemical interfaces. We tried to apply electrochemical potentials within the range of −1 to 1 V vs the Ag/AgCl reference electrode. However, we observed no C≡N stretch Raman signal of this molecule under positive potentials, which suggests that this molecularly functionalized surface is only stable under reducing potentials but not oxidative potentials. After we obtained the Raman spectra, we fitted the peaks using a Lorentzian function and plotted the Raman frequency of the C≡N stretch as a function of the reference potential.

RESULTS AND DISCUSSION

Figure 2a shows the SERS-enhanced Raman spectra of the napthyl nitrile-functionalized Si in DI water under various applied potentials, as indicated in the legend. Here, we observe a red shift in the vibrational frequency of the C≡N stretch of the napthyl nitrile under negative applied potentials due to the local electric fields produced at the silicon−aqueous interface. Since the raw data is not clear enough, we also plot the zoomed-in version of fitted spectra in the inset of Figure 2a. The vibrational frequency of the C≡N stretch is known to be particularly sensitive to applied electric fields. Figure 2b shows the Raman shift of this vibrational mode plotted as a function of reference potential. Here, we observe a 4.7 cm^{-1} red shift over the applied voltage range, which is in the same order of Stark shifts as observed in our previous work on metal electrodes.[17,18,37]

Figure 3 shows the SERS-enhanced Raman spectra of the napthyl nitrile-functionalized Si in 0.1 M KCl under various applied potentials. Again, we observe a red shift in the vibrational frequency of the C≡N stretch of the napthyl nitrile

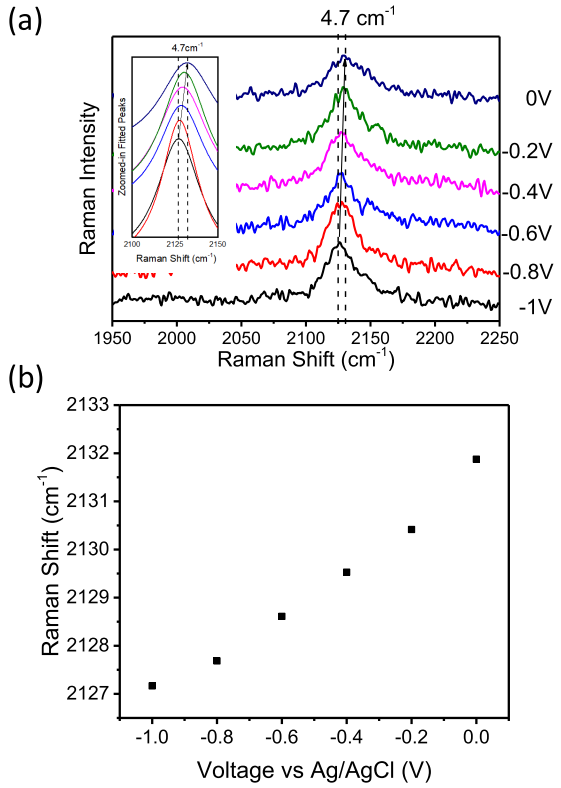

Figure 2. (a) Waterfall plot of the raw Raman spectra of napthyl nitrile-functionalized Si in DI water under various applied potentials as indicated in the legend, the zoomed-in fitted peaks in the inset plot, (b) Raman shift of the nitrile stretch plotted as a function of the applied electrochemical potential.

under negative applied potentials due to the local electric fields produced at the silicon−aqueous interface. Since the raw data is not clear enough, we also plot the zoomed-in version of fitted spectra in the inset of Figure 3a. Figure 3b shows the Raman shift of this vibrational mode plotted as a function of reference potential in both DI water and 0.1 M KCl. In KCl, we observe an 8.6 cm^{-1} downshift over the applied voltage range, which is somewhat larger than that observed in the DI water due to the higher ionic strength of the KCl solution.[17,18]

To convert the experimentally observed Stark shift to the electric field strength, the napthyl nitrile molecule, which functionalizes Si is modeled. The oxygen atom, which is bonded on Si is capped with a hydrogen atom in the simulation. The carbon−carbon double bond, which connects to the nitrile group is aligned in the direction where the electric fields are applied. The factor used to convert the field strength unit is 1 au = 5.14 × 10^9 V/cm.[41] Full geometry optimization and frequency calculations of the molecule were performed under different electric fields. All calculations in this work were performed using a local version of the Amsterdam density functional (ADF) program package.[42,43] The Becke−Perdew (BP86) XC-potential[44,45] and triple ζ-polarized (TZP) slater-type basis set with large frozen cores from the ADF basis set library were used. The vibrational frequencies and normal modes were calculated within the harmonic approximation. The vibrational frequencies of nitrile stretching are plotted against the electric field strength in Figure 4. The slope of the fitted line predicts a Stark tuning rate (STR) of 0.5622 (cm^{-1})/(MV cm^{-1}).

https://dx.doi.org/10.1021/acs.jpcc.0c03966
J. Phys. Chem. C 2020, 124, 17000−17005

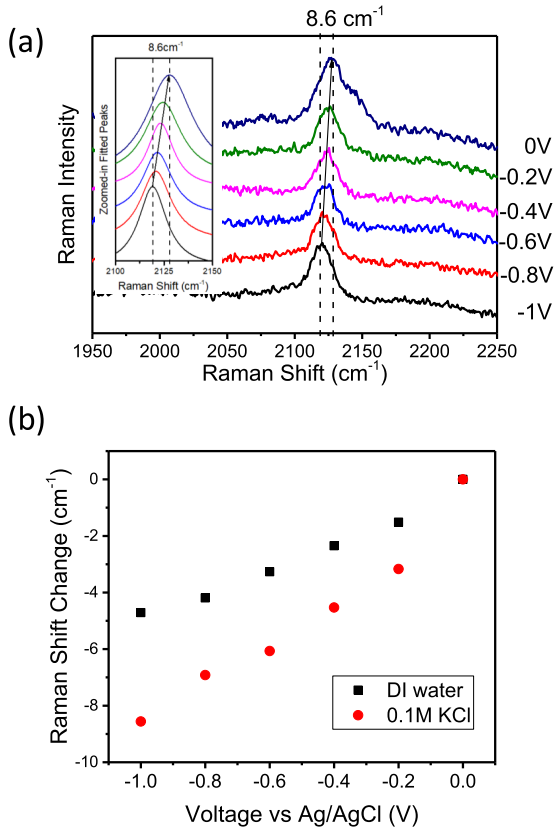

Figure 3. (a) Waterfall plot of the raw Raman spectra of napthyl nitrile-functionalized Si in 0.1 M KCl solution under various applied potentials as indicated in the legend measured, the zoomed-in fitted peaks in the inset plot and (b) Raman shift of the nitrile stretch plotted as a function of the applied electrochemical potential in DI water and 0.1 M KCl solution.

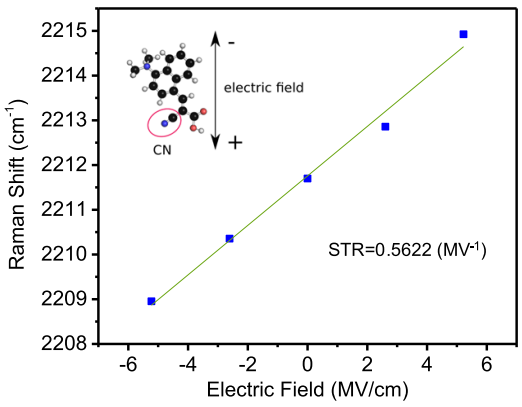

Figure 4. Raman shift of the nitrile stretch plotted as a function of the local electric field obtained by calculation.

Based on this calculated Stark tuning rate, we converted the Raman red shifts observed in DI water and a KCl solution to the electric field, as plotted in Figure 5. Here, the observed Stark shifts correspond to electric fields in excess of −10 MV/cm. This negative field points down toward the silicon surface and plays an important role in reduction processes, such as the hydrogen evolution reaction (HER) by driving positively charged ions (e.g., H^+) to the surface, where they can undergo charge transfer with the underlying substrate.

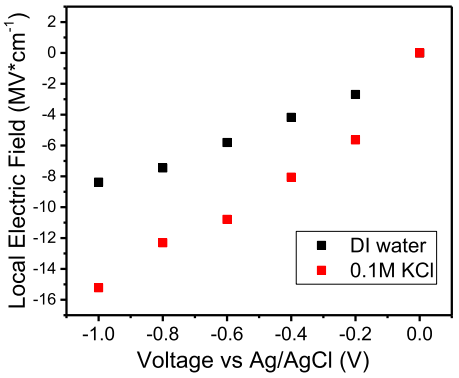

Figure 5. Local electric field plotted as a function of the applied electrochemical potential in different liquid environments as indicated in the legend.

CONCLUSIONS

In conclusion, spectroscopic measurements of the electrostatic field produced at the surface of an electrochemical semiconductor−electrolyte interface are reported using vibrational Stark shifts of napthyl nitrile-functionalized silicon. The vibrational frequency of the C≡N bond is sensitive to electric fields and, therefore, provides a mechanism for monitoring the electric fields that occur at the semiconductor−electrolyte interface. In DI water and KCl solutions, the nitrile (i.e., C≡N) stretch red shifts by 4.7 and 8.6 cm^{-1} at an applied potential of −1 V vs Ag/AgCl. First principles calculations of the napthyl nitrile complex are carried out as a function of the electric field, yielding a Stark tuning rate (STR) of 0.5622 $cm^{-1}/(MV\ cm^{-1})$. This STR is used to convert the measured Stark shifts to *E*-field, yielding maximum *E*-fields of −8.4 and −15.2 MV/cm at −1 V vs Ag/AgCl. These electric fields are responsible for driving positively charged ions and reactants to the surface where they can undergo electron transfer from the underling silicon in fulfillment of the reduction process.

AUTHOR INFORMATION

Corresponding Author

Stephen B. Cronin − *Department of Chemistry and Ming Hsieh Department of Electrical Engineering, University of Southern California, Los Angeles, California 90089, United States;* orcid.org/0000-0001-9153-7687; Email: scronin@usc.edu

Authors

Haotian Shi − *Department of Chemistry, University of Southern California, Los Angeles, California 90089, United States*

Ryan T. Pekarek − *Chemistry and Nanoscience Center, National Renewable Energy Laboratory, Golden, Colorado 80401, United States*

Ran Chen − *Department of Chemistry, Pennsylvania State University, University Park, Pennsylvania 16802, United States*

Boxin Zhang − *Department of Materials Science, University of Southern California, Los Angeles, California 90089, United States*

Yu Wang − *Department of Materials Science, University of Southern California, Los Angeles, California 90089, United States;* orcid.org/0000-0002-0307-1301

Indu Aravind − *Ming Hsieh Department of Electrical Engineering, University of Southern California, Los Angeles, California 90089, United States*

https://dx.doi.org/10.1021/acs.jpcc.0c03966
J. Phys. Chem. C 2020, 124, 17000−17005

Zhi Cai − *Department of Materials Science, University of Southern California, Los Angeles, California 90089, United States*

Lasse Jensen − *Department of Chemistry, Pennsylvania State University, University Park, Pennsylvania 16802, United States;* orcid.org/0000-0003-1237-5021

Nathan R. Neale − *Chemistry and Nanoscience Center, National Renewable Energy Laboratory, Golden, Colorado 80401, United States;* orcid.org/0000-0001-5654-1664

Complete contact information is available at: https://pubs.acs.org/10.1021/acs.jpcc.0c03966

Notes

The authors declare no competing financial interest.

■ ACKNOWLEDGMENTS

This research was supported by the National Science Foundation (NSF) award no. 1708581 (H.S.) and CBET-1512505 (B.Z.), the Army Research Office (ARO) award no. W911NF-17-1-0325 (Y.W.), the Air Force Office of Scientific Research (AFOSR) grant no. FA9550-19-1-0115 (I.A.), and the Department of Energy (DOE) award no. DE-SC0019322 (Z.C.). L.J. and R.C. acknowledge the support from the National Science Foundation Grant CHE-1707657. Portions of this work were conducted with Advanced Cyberinfrastructure computational resources provided by the Institute for Cyber-Science at the Pennsylvania State University (https://ics.psu.edu/). This work was conducted in part by the Alliance for Sustainable Energy, LLC, the manager and operator of the National Renewable Energy Laboratory for the U.S. Department of Energy (DOE) under Contract no. DE-AC36-08GO28308. Funding for molecular functionalization of a silicon surface and paper preparation was provided by the U.S. DOE, Office of Science, Office of Basic Energy Sciences, Division of Chemical Sciences, Geosciences, and Biosciences, Solar Photochemistry Program. The views expressed in the article do not necessarily represent the views of the DOE or the U.S. government. The publisher, by accepting the article for publication, acknowledges that the U.S. government retains a nonexclusive, paid-up, irrevocable, worldwide license to publish or reproduce the published form of this work, or allow others to do so, for U.S. government purposes.

■ REFERENCES

(1) Fujishima, A.; Honda, K. Electrochemical Photolysis of Water at a Semiconductor Electrode. *Nature* **1972**, *238*, 37−38.

(2) Inoue, T.; Fujishima, A.; Konishi, S.; Honda, K. Photoelectrocatalytic Reduction of Carbon Dioxide in Aqueous Suspensions of Semiconductor Powders. *Nature* **1979**, *277*, 637−638.

(3) Chen, Y. W.; Prange, J. D.; Duhnen, S.; Park, Y.; Gunji, M.; Chidsey, C. E. D.; McIntyre, P. C. Atomic Layer-Deposited Tunnel Oxide Stabilizes Silicon Photoanodes for Water Oxidation. *Nat. Mater.* **2011**, *10*, 539−544.

(4) Frese, K., Jr; Madou, M.; Morrison, S. Investigation of Photoelectrochemical Corrosion of Semiconductors. *J. Phys. Chem. A* **1980**, *84*, 3172−3178.

(5) Qiu, J.; Zeng, G.; Pavaskar, P.; Li, Z.; Cronin, S. B. Plasmon-Enhanced Water Splitting on TiO_2-Passivated GaP Photocatalysts. *Phys. Chem. Chem. Phys.* **2014**, *16*, 3115.

(6) Zeng, G.; Qiu, J.; Pavaskar, P.; Li, Z.; Cronin, S. B. CO_2 Reduction to Methanol on TiO_2-Passivated GaP Photocatalysts. *ACS Catal.* **2014**, *4*, 3512.

(7) Lee, M. H.; Takei, K.; Zhang, J. J.; Kapadia, R.; Zheng, M.; Chen, Y. Z.; Nah, J.; Matthews, T. S.; Chueh, Y. L.; Ager, J. W.; et al. p-Type InP Nanopillar Photocathodes for Efficient Solar-Driven Hydrogen Production. *Angew. Chem., Int. Ed.* **2012**, *51*, 10760−10764.

(8) Hu, S.; Shaner, M. R.; Beardslee, J. A.; Lichterman, M.; Brunschwig, B. S.; Lewis, N. S. Amorphous TiO_2 Coatings Stabilize Si, GaAs, and GaP Photoanodes for Efficient Water Oxidation. *Science* **2014**, *344*, 1005−1009.

(9) Bonke, S. A.; Wiechen, M.; MacFarlane, D. R.; Spiccia, L. Renewable Fuels from Concentrated Solar Power: Towards Practical Artificial Photosynthesis. *Energy Environ. Sci.* **2015**, *8*, 2791−2796.

(10) Döscher, H.; Young, J. L.; Geisz, J. F.; Turner, J. A.; Deutsch, T. G. Solar-to-Hydrogen Efficiency: Shining Light on Photoelectrochemical Device Performance. *Energy Environ. Sci.* **2016**, *9*, 74−80.

(11) Young, J. L.; Steiner, M. A.; Döscher, H.; France, R. M.; Turner, J. A.; Deutsch, T. G. Direct Solar-to-Hydrogen Conversion via Inverted Metamorphic Multi-Junction Semiconductor Architectures. *Nat. Energy* **2017**, *2*, No. 17028.

(12) Cheng, W.-H.; Richter, M. H.; May, M. M.; Ohlmann, J.; Lackner, D.; Dimroth, F.; Hannappel, T.; Atwater, H. A.; Lewerenz, H.-J. Monolithic Photoelectrochemical Device for Direct Water Splitting with 19% Efficiency. *ACS Energy Lett.* **2018**, *3*, 1795−1800.

(13) Salvador, P. Hole Diffusion Length in N-TiO_2 Single-Crystals and Sintered Electrodes- Photoelectrochemical Determination and Comparative-Analysis. *J. Appl. Phys.* **1984**, *55*, 2977−2985.

(14) Fujishima, A.; Honda, K. Electrochemical Photolysis of Water at a Semiconductor Electrode. *Nature* **1972**, *238*, 37.

(15) Hu, S.; Chi, C. Y.; Fountaine, K. T.; Yao, M. Q.; Atwater, H. A.; Dapkus, P. D.; Lewis, N. S.; Zhou, C. W. Optical, Electrical, and Solar Energy-Conversion Properties of Gallium Arsenide Nanowire-Array Photoanodes. *Energy Environ. Sci.* **2013**, *6*, 1879−1890.

(16) Zaban, A.; Ferrere, S.; Gregg, B. A. Relative Energetics at the Semiconductor/Sensitizing Dye/Electrolyte Interface. *J. Phys. Chem. B* **1998**, *102*, 452−460.

(17) Sorenson, S. A.; Patrow, J. G.; Dawlaty, J. M. Solvation Reaction Field at the Interface Measured by Vibrational Sum Frequency Generation Spectroscopy. *J. Am. Chem. Soc.* **2017**, *139*, 2369−2378.

(18) Patrow, J. G.; Sorenson, S. A.; Dawlaty, J. M. Direct Spectroscopic Measurement of Interfacial Electric Fields near an Electrode under Polarizing or Current-Carrying Conditions. *J. Phys. Chem. C* **2017**, *121*, 11585−11592.

(19) Ge, A.; Videla, P. E.; Lee, G. L.; Rudshteyn, B.; Song, J.; Kubiak, C. P.; Batista, V. S.; Lian, T. Interfacial Structure and Electric Field Probed by in Situ Electrochemical Vibrational Stark Effect Spectroscopy and Computational Modeling. *J. Phys. Chem. C* **2017**, *121*, 18674−18682.

(20) Schkolnik, G.; Salewski, J.; Millo, D.; Zebger, I.; Franzen, S.; Hildebrandt, P. Vibrational Stark Effect of the Electric-Field Reporter 4-Mercaptobenzonitrile as a Tool for Investigating Electrostatics at Electrode/SAM/Solution Interfaces. *Int. J. Mol. Sci.* **2012**, *13*, 7466−7482.

(21) Oklejas, V.; Sjostrom, C.; Harris, J. M. SERS Detection of the Vibrational Stark Effect from Nitrile-Terminated SAMs to Probe Electric Fields in the Diffuse Double-Layer. *J. Am. Chem. Soc.* **2002**, *124*, 2408−2409.

(22) Oklejas, V.; Sjostrom, C.; Harris, J. M. Surface-Enhanced Raman Scattering Based Vibrational Stark Effect as a Spatial Probe of Interfacial Electric Fields in the Diffuse Double Layer. *J. Phys. Chem. B* **2003**, *107*, 7788−7794.

(23) Kumar, R.; Zhou, H.; Cronin, S. B. Surface-Enhanced Raman Spectroscopy and Correlated Scanning Electron Microscopy of Individual Carbon Nanotubes. *Appl. Phys. Lett.* **2007**, *91*, No. 223105.

(24) Kneipp, K.; Kneipp, H.; Corio, P.; Brown, S. D. M.; Shafer, K.; Motz, J.; Perelman, L. T.; Hanlon, E. B.; Marucci, A.; Dresselhaus, G.; et al. Surface-Enhanced and Normal Stokes and Anti-Stokes Raman Spectroscopy of Single-Walled Carbon Nanotubes. *Phys. Rev. Lett.* **2000**, *84*, 3470−3473.

(25) Liu, Z.; Hou, W.; Pavaskar, P.; Aykol, M.; Cronin, S. B. Plasmon Resonant Enhancement of Photocatalytic Water Splitting Under Visible Illumination. *Nano Lett.* **2011**, *11*, 1111−1116.
(26) Pavaskar, P.; Theiss, J.; Cronin, S. B. Plasmonic Hot Spots: Nanogap Enhancement vs. Focusing Effects from Surrounding Nanoparticles. *Opt. Express* **2012**, *20*, 14656−14662.
(27) Pavaskar, P.; Hsu, I. K.; Theiss, J.; Hsuan Hung, W.; Cronin, S. B. A Microscopic Study of Strongly Plasmonic Au and Ag Island Thin Films. *J. Appl. Phys.* **2013**, *113*, No. 034302.
(28) Harroun, S. G.; Abraham, T. J.; Prudhoe, C.; Zhang, Y.; Scammells, P. J.; Brosseau, C. L.; Pye, C. C.; Singer, R. D. Electrochemical Surface-Enhanced Raman Spectroscopy (E-SERS) of Novel Biodegradable Ionic Liquids. *Phys. Chem. Chem. Phys.* **2013**, *15*, 19205−19212.
(29) Kudelski, A.; Pettinger, B. Fluctuations of Surface-Enhanced Raman Spectra of CO Adsorbed on Gold Substrates. *Chem. Phys. Lett.* **2004**, *383*, 76−79.
(30) Sanchez, L. A.; Birke, R. L.; Lombardi, J. R. Surface-Enhanced Raman Scattering of Piperidine. The effect of electrode potential on intensity. *J. Phys. Chem. A.* **1984**, *88*, 1762−1766.
(31) Abdelsalam, M.; Bartlett, P. N.; Russell, A. E.; Baumberg, J. J.; Calvo, E. J.; Tognalli, N. G.; Fainstein, A. Quantitative Electrochemical SERS of Flavin at a Structured Silver Surface. *Langmuir* **2008**, *24*, 7018−7023.
(32) Xu, H.; Xie, L.; Zhang, H.; Zhang, J. Effect of Graphene Fermi Level on the Raman Scattering Intensity of Molecules on Graphene. *ACS Nano* **2011**, *5*, 5338−5344.
(33) Sriram, S.; Bhaskaran, M.; Chen, S.; Jayawardhana, S.; Stoddart, P. R.; Liu, J. Z.; Medhekar, N. V.; Kalantar-Zadeh, K.; Mitchell, A. Influence of Electric Field on SERS: Frequency Effects, Intensity Changes, and Susceptible Bonds. *J. Am. Chem. Soc.* **2012**, *134*, 4646−4653.
(34) Buriak, J. M. Functionalization of Silicon Surfaces for Device Applications. *J. Lab. Autom.* **1999**, *4*, 36−39.
(35) Buriak, J. M. Organometallic Chemistry on Silicon and Germanium Surfaces. *Chem. Rev.* **2002**, *102*, 1271−1308.
(36) Gonçales, V. R.; Lian, J.; Gautam, S.; Tilley, R. D.; Gooding, J. J. Functionalized Silicon Electrodes in Electrochemistry. *Annu. Rev. Anal. Chem.* **2020**, *13*, 135−158.
(37) Shi, H.; Cai, Z.; Patrow, J.; Zhao, B.; Wang, Y.; Wang, Y.; Benderskii, A.; Dawlaty, J.; Cronin, S. B. Monitoring Local Electric Fields at Electrode Surfaces Using Surface Enhanced Raman Scattering-Based Stark-Shift Spectroscopy during Hydrogen Evolution Reactions. *ACS Appl. Mater. Interfaces* **2018**, *10*, 33678−33683.
(38) Shi, H.; Zhao, B.; Ma, J.; Bronson, M. J., Jr; Cai, Z.; Chen, J.; Wang, Y.; Cronin, M.; Jensen, L.; Cronin, S. B. Measuring Local Electric Fields and Local Charge Densities at Electrode Surfaces Using Graphene-Enhanced Raman Spectroscopy (GERS)-Based Stark-Shifts. *ACS Appl. Mater. Interfaces* **2019**, *11*, 36252−36258.
(39) Kroupa, D. M.; Vörös, M.; Brawand, N. P.; Bronstein, N.; McNichols, B. W.; Castaneda, C. V.; Nozik, A. J.; Sellinger, A.; Galli, G.; Beard, M. C. Optical Absorbance Enhancement in PbS QD/Cinnamate Ligand Complexes. *J. Phys. Chem. Lett.* **2018**, *9*, 3425−3433.
(40) Liu, Z.; Hou, W.; Pavaskar, P.; Aykol, M.; Cronin, S. Plasmon Resonant Enhancement of Photocatalytic Water Splitting Under Visible Illumination. *Nano Lett.* **2011**, *11*, 1111.
(41) The NIST Reference on Constants, Units, and Uncertainty, 2019.
(42) Te Velde, G.; Bickelhaupt, F. M.; Baerends, E. J.; Fonseca Guerra, C.; Van Gisbergen, S. J. A.; Snijders, J. G.; Ziegler, T. Chemistry with ADF. *J. Comput. Chem.* **2001**, *22*, 931−967.
(43) Baerends, E. J.; Atkins, A. J.; Autschbach, J.; Bashford, D.; Baseggio, O.; Bérces, A. F. M.; Bickelhaupt, C.; Boerritger, P. M.; Cavallo, L.; Paul, C. et al. ADF2018,Theoretical Chemistry. 2018, http://www.scm.com.
(44) Becke, A. D. Density-Functional Exchange-Energy Approximation with Correct Asymptotic Behavior. *Phys. Rev. A* **1988**, *38*, 3098−3100.
(45) Perdew, J. P. Density-Functional Approximation for the Correlation Energy of the Inhomogeneous Electron Gas. *Phys. Rev. B* **1986**, *33*, 8822−8824.

https://dx.doi.org/10.1021/acs.jpcc.0c03966
J. Phys. Chem. C 2020, 124, 17000−17005